

Learning Compact Channel Correlation Representation for LiDAR Place Recognition

Saimunur Rahman¹, Peyman Moghadam^{1,2}

Abstract—This paper presents a novel approach to learn compact channel correlation representation for LiDAR place recognition, called *C3R*, aimed at reducing the computational burden and dimensionality associated with traditional covariance pooling methods for place recognition tasks. Our method partitions the feature matrix into smaller groups, computes group-wise covariance matrices, and aggregates them via a learnable aggregation strategy. Matrix power normalization is applied to ensure stability. Theoretical analyses are also given to demonstrate the effectiveness of the proposed method, including its ability to preserve permutation invariance and maintain high mutual information between the original features and the aggregated representation. We conduct extensive experiments on four large-scale, public LiDAR place recognition datasets including Oxford RobotCar, In-house, MulRan, and WildPlaces datasets to validate our approach’s superiority in accuracy, and robustness. Furthermore, we provide the quantitative results of our approach for a deeper understanding. The code will be released upon acceptance.

I. INTRODUCTION

LiDAR place recognition (LPR), the task of estimating previously visited places when traversing an environment, plays an important role for robotic and autonomous systems navigation, and Simultaneous Localisation and Mapping (SLAM) [1], [2]. LPR generally involves extracting features from LiDAR point clouds and comparing these features with those stored in a database for establishing correspondences with an appropriate similarity metric such as Euclidean distance. The aim is to recognize places even under continuous environmental conditions changes such as weather, lighting or viewpoint variations.

Feature pooling is mandatory in LPR methods as it combines and compresses the extracted local features from input point clouds with varying numbers of points to a fixed-size global descriptor per input pointcloud, reducing the dimensionality without sacrificing the relevant information for recognition. Traditional pooling methods used in LPR such as average pooling, max pooling, GeM pooling [7] and NetVLAD pooling [8] give computationally efficient yet effective mechanisms for reducing the dimension. These methods are also known as first-order pooling methods [9], [10] and they are limited in terms of their capacity to capture complex relationships in the features [11]. They dampen the most informative features, leading to a phenomenon known as “feature burstiness”, where discriminative details

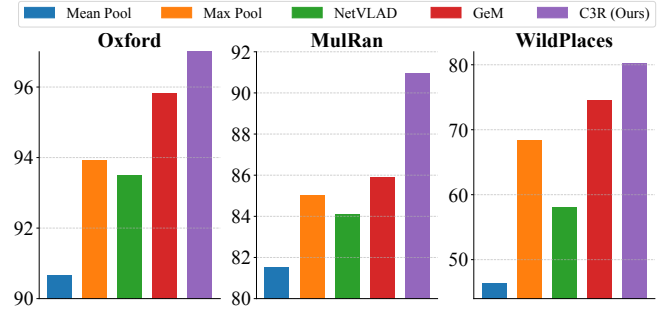


Fig. 1: Effectiveness of our *C3R* over popular LPR pooling methods on Oxford RobotCar [3], MulRan (Sejong environment) [4] and WildPlaces (Venman environment) [5] datasets. All methods used MinkLoc3Dv2 [6] features and evaluated on a single GPU. Compared in terms of Recall@1.

are diluted. These methods do not consider feature interactions, making them less effective in distinguishing between important details and irrelevant background noise, resulting in weaker performance. In contrast, second-order pooling methods such as covariance pooling [10] capture complex feature relationships by going beyond first-order pooling, offering a much richer and discriminative representation suitable for robust LPR. They are less sensitive to the background (*e.g.*, points from the surface of roads in urban scenarios). Despite their potential, these methods compute the full covariance matrix of features, which is high-dimensional and computationally burdensome, making them unsuitable for real-world robotic applications and large-scale environments. Furthermore, they significantly increase the database search time causing delays in LPR systems [8]. How to effectively reduce the dimensionality of second-order pooling methods for LPR tasks is a relatively under-explored area in literature.

To answer this question, we propose a Compact Channel Correlation Representation (*C3R*), that produces compact covariance matrices by leveraging the idea of channel partitioning. Specifically, instead of computing a full covariance matrix from the entire feature set as done in the existing methods, we partition the feature channels into smaller equal-sized groups, each forming smaller covariance matrices. These group-wise covariance matrices effectively capture local feature component correlations, which are then aggregated using a learnable weighted sum. This approach significantly reduces the dimensionality burden while keeping important information from each group, resulting representation that remains discriminative. Moreover, by focusing

¹ CSIRO Robotics, DATA61, CSIRO, Australia. E-mails: *firstname.lastname@csiro.au*

² School of Electrical Engineering and Robotics, Queensland University of Technology (QUT), Brisbane, Australia.

on smaller, manageable covariance matrices, *C3R* enables faster database searches in large-scale LPR tasks. It keeps the advantage of second-order pooling – capturing rich feature correlations, without the computational burdens typically associated with full covariance matrix computation.

In comparison with the pooling method of LoGG3D-net [12], which does not inherently produce a smaller covariance matrix but instead reduces the feature dimensions for obtaining smaller covariance matrices, our method produces a compact representation instead of a full covariance representation directly. In addition, we are scalable to large feature channels with a negligible computation cost. We are also significantly better than NetVLAD pooling [8] popularly used in LPR in terms of both the size of learnable parameters and performance, as illustrated in Figure 1 where we compare against other pooling methods. Furthermore, our proposed method is invariant to point permutations.

We conduct extensive experiments with our proposed method on four popular LPR datasets, namely, Oxford Robotcar [3], In-house [8], MulRan [4] and WildPlaces [5], to demonstrate its effectiveness. We also compare with the existing state-of-the-art, common first-order pooling methods used in LPR and two popular covariance pooling methods from the image domain [9], [13].

II. RELATED WORKS

The main focus of our paper is LPR. While we acknowledge the contributions of pioneering methods such as PatchNetVLAD [14], MixVPR [15], and SALAD [16] in Visual Place Recognition (VPR), these methods primarily operate in 2D vision. Given the unique challenges posed by sparse point clouds and the varying input sizes in LPR, further investigation is needed to determine the applicability and effectiveness of these methods in the context of LPR.

First-order Methods are widely used in most LPR methods [8], [17]–[22]. PointNetVLAD [8] pioneered the 3D feature pooling by integrating NetVLAD [23] with PointNet [24]. To tackle the high-dimensional output produced by NetVLAD, it used linear projection. Although it gives a good performance, the linear projection and NetVLAD operations such as clustering produce large learnable parameters which may occasionally lead to overfitting in low data scenarios. Another popular pooling method for LPR is Generalized Mean (GeM) pooling [25], [26]. Despite its good results and compact representation, GeM [7] can be sensitive to outliers typically observed in point clouds that are captured in unstructured environments such as the WildPlaces dataset [5]. Furthermore, it has a single learnable parameter that controls its behavior which reduces its flexibility with diverse point clouds and tasks. Orthogonal to these methods, some works used global max pooling (*e.g.*, [27]) and global average pooling (*e.g.*, [28]) and leveraged cross-attention to further improve their performance.

Unlike PointNetVLAD, we do not apply linear projection in our method as it produces compact representation by default. Also, each group-wise smaller covariance matrix in our method is regularized with independent learnable

parameters, therefore, unlike GeM, our method offers more flexibility in the learned representation.

Second-order Methods have been widely used in 2D vision, particularly for fine-grained tasks [29], [30]. Bilinear CNN [31] is among the first to combine covariance matrix as a pooling mechanism with CNNs and to conduct end-to-end training. Improved Bilinear [10] and MPN-COV [32] made further improvements to it. Meanwhile, compact covariance pooling methods such as CBP [9] are also developed to produce compact and discriminative covariance representation since Bilinear CNN produces large dimensional features. They primarily use low-rank projections of full covariance matrices to produce lower dimensional features. However, in terms of performance, these methods perform poorly than the full covariance matrix based methods due to their reduced dimension. Recent developments such as [13], [33], have made attempts to improve this limitation.

The use of the second-order method in LPR can be traced back to Locus [34], which employs covariance pooling of individual point descriptors and then selects the maximum of entries from the computed covariance matrices. Later, LoGG3D-Net [12] integrated this idea with a sparse U-Net network and a local constancy loss for end-to-end training. While it achieved impressive performance LPR, its major drawback is the requirement of large memory to store the point descriptor-wise covariance matrices, which increases linearly with the size of the point cloud. However, LoGG3D-Net avoids this issue by using a relatively small number of feature channels when computing the second-order representation. In contrast, most LPR networks produce significantly higher feature channels (*e.g.*, 16 vs. 256), which could cause memory overflow issues if the above pooling method is applied.

In comparison, our proposed approach requires significantly less memory to store covariance matrices, as we compute one channel-wise covariance matrix. Furthermore, we employ a GPU-compatible matrix normalization method that does not suffer from the numerical instabilities present in their approach. Finally, our method naturally produces a much more compact representation without needing to reduce the number of feature channels. In addition, we do not use complex mechanisms such as projections as in compact covariance pooling methods which often require hyperparameter tuning and architectural changes in frameworks, therefore, our method can be easily integrated into deep networks than those methods.

III. METHODOLOGY

Fig. 2 gives an overview of our proposed method. Given point cloud $\mathbf{P} \in \mathbb{R}^{n \times 3}$ where n is the number of points, we first extract its features in the form of a matrix $\mathbf{F} \in \mathbb{R}^{d \times n'}$ by passing it through an encoder network. d is the number of feature channels and n' is the reduced points after convolution operations. Generally, $n' \ll n$ unless an encoder-decoder network is used, *e.g.*, [12]. The goal of our method is to summarise \mathbf{F} into a compact second-order global representation.

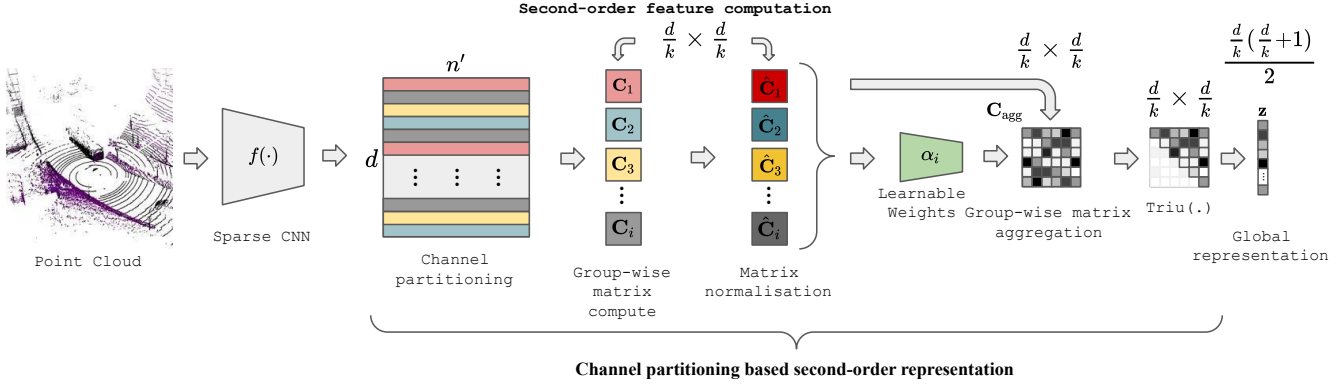


Fig. 2: Overview of our C3R method. Given a point cloud, we extract its features with a sparse CNN-based encoder network $f(\cdot)$. We then partition the channels into equal groups. For each group, we compute a separate covariance matrix, followed by a matrix normalization operation. We then aggregate these group-wise normalized matrices into a single matrix with proposed aggregation strategies. Finally, we take the upper triangular entries of the final matrix as a global representation.

A. Problem Formulation

The conventional approach to covariance pooling [10], [32] computes a full covariance matrix $\mathbf{C} \in \mathbb{R}^{d \times d}$ as:

$$\mathbf{C} = \frac{1}{n-1}(\mathbf{F} - \mu)(\mathbf{F} - \mu)^\top, \quad (1)$$

where μ is the mean vector of the features \mathbf{F} . While this matrix captures rich second-order information, its dimensionality $d \times d$ becomes impractically large as d increases, leading to high computational costs. This could potentially cause issues during its deployment on robots in real-world scenarios, which have limited memory and computation resources.

To address this issue, we propose partitioning the feature matrix \mathbf{F} into k non-overlapping groups, where each group $\mathbf{F}_i \in \mathbb{R}^{\frac{d}{k} \times n}$ consists of $\frac{d}{k}$ feature channels. The full feature matrix can be expressed as the concatenation of these groups:

$$\mathbf{F} = [\mathbf{F}_1; \mathbf{F}_2; \dots; \mathbf{F}_k]. \quad (2)$$

A smaller covariance matrix $\mathbf{C}_i \in \mathbb{R}^{\frac{d}{k} \times \frac{d}{k}}$ is computed from each group \mathbf{F}_i , defined as:

$$\mathbf{C}_i = \frac{1}{n-1}(\mathbf{F}_i - \mu_i)(\mathbf{F}_i - \mu_i)^\top, \quad (3)$$

where μ_i is the mean vector of the group \mathbf{F}_i . In comparison with the full covariance matrices, the smaller covariance matrices have significantly lower computational complexity and memory requirements, *i.e.*, $\frac{d}{k} \times \frac{d}{k} \ll d \times d$.

B. Normalization of Covariance Matrices

Since covariance matrices lie in the manifold of symmetric positive definite (SPD) matrices, normalization is needed for projecting them to the Euclidean space for facilitating routine operations such as computation of loss for conducting the training process. Besides that, it also improves the covariance matrices in terms of their reliability and ability to deal with feature burstiness [32], [35].

We apply normalization of each group-wise covariance matrix \mathbf{C}_i using matrix power normalization (MPN) [10], [32]. As opposed to the conventional approach of applying MPN using eigen-decomposition¹ which has poor GPU support and numerical instability issues [10], [36], we use Newton-Schulz iteration [37] for accelerated and stable normalization operation with GPU. The process is discussed below.

For simplicity in our discussion, let us denote the smaller covariance matrices \mathbf{C}_i from the previous step with \mathbf{A} . Given $\mathbf{Y}_0 = \mathbf{A}$ and $\mathbf{Z}_0 = \mathbf{I}$, the Newton-Schulz iteration performs the square root of \mathbf{A} , *i.e.*, $\mathbf{Y} = \mathbf{A}^{1/2}$, by iterating the Eq. (4) for l iterations in a sequential closed-loop manner:

$$\begin{aligned} \mathbf{Y}_l &= \frac{1}{2}\mathbf{Y}_{l-1}(3\mathbf{I} - \mathbf{Z}_{l-1}\mathbf{Y}_{l-1}) \\ \mathbf{Z}_l &= \frac{1}{2}(3\mathbf{I} - \mathbf{Z}_{l-1}\mathbf{Y}_{l-1})\mathbf{Z}_{l-1}. \end{aligned} \quad (4)$$

However, Eq. (4) only converges locally when $\|\mathbf{A} - \mathbf{I}\|_2 < 0$. To satisfy this criteria, we normalise \mathbf{A} with its trace, *i.e.*, $\mathbf{A} = \mathbf{A}/\text{trace}(\mathbf{A})$. Since this changes the data magnitudes non-trivially, it affects the convergence of the network. To remedy this, we apply following compensation: $\mathbf{Y} = \sqrt{\text{trace}(\mathbf{A})}\mathbf{Y}_l$. \mathbf{Y} is a well-conditioned SPD matrix and has balanced eigenvalues which is essential for stable aggregation of group covariance matrices for LPR tasks. For clarity, we now denote \mathbf{A} for \mathbf{C}_i and \mathbf{Y} for $\hat{\mathbf{C}}_i$ to represent the MPN operation.

C. Aggregation of Group Covariance Matrices

At this step, we aggregate normalized group-wise covariance matrices $\hat{\mathbf{C}}_i$ into a single covariance matrix \mathbf{C}_{agg}

¹Given a covariance matrix \mathbf{C} traditional approach of MPN is defined as $\mathbf{C}^{\frac{1}{2}} = \mathbf{U}\mathbf{D}^{\frac{1}{2}}\mathbf{U}^\top$, where \mathbf{U} and \mathbf{D} are the eigenvectors and eigenvalues of \mathbf{C} , respectively. The gradients are computed as $\delta\mathbf{C}^{\frac{1}{2}} = \mathbf{U}(\mathbf{L}^\top \circ (\mathbf{U}^\top \delta\mathbf{U}))\mathbf{U}^\top$, where l_{ij} is defined as $1/(\lambda_i - \lambda_j)$ when $i \neq j$ and 0 otherwise. [36] provides a comprehensive discussion on computational instability of this operation.

to achieve a lower-dimensional covariance representation. Instead of simply concatenating them (e.g., [38]) which will lead to a large dimensional global representation, we use the following simple yet effective strategy since our goal is to compute compact covariance representation.

We compute a weighted sum of the normalized covariance matrices, where the weights α_i are normalized with softmax(\cdot) operator and that their sum equals 1 and are learned in an end-to-end manner:

$$\mathbf{C}_{\text{agg}} = \sum_{i=1}^k \alpha_i \hat{\mathbf{C}}_i; \quad \alpha_i = \frac{\exp(\alpha_i)}{\sum_{j=1}^k \exp(\alpha_j)}, \quad (5)$$

where α_i represent the weight of $\hat{\mathbf{C}}_i$. We initialize α uniformly by setting α_i to a constant value derived from the uniform distribution over the range [0, 1]. Specifically, initialize each weight α_i to 1, which corresponds to setting $\alpha_i \sim \text{uniform}(1)$ for $i = 1, 2, \dots, k$. This initialization ensures that all weights start with the same value and are optimized during training to allow the model to automatically adjust the importance of each group during training.

Final Representation: Since \mathbf{C}_{agg} is a symmetric matrix, can we only take its upper-triangular entries and discard the rest to form a vectorized representation $\mathbf{z} = \text{triu}(\mathbf{C}_{\text{agg}})$ which further reduces the dimension of \mathbf{C}_{agg} from $\frac{d}{k} \times \frac{d}{k}$ to $\frac{\frac{d}{k} + (\frac{d}{k} + 1)}{2}$, i.e., $\frac{\frac{d}{k} + (\frac{d}{k} + 1)}{2} \ll \frac{d}{k} \times \frac{d}{k} \ll d \times d$ when $k > 1$.

D. Theoretical Explanation

From information-theoretic standpoint, our method viewed as mutual information $\mathbf{I}(\mathbf{F}; \mathbf{C}_{\text{agg}})$ maximization between the \mathbf{F} and \mathbf{C}_{agg} . Mutual information quantifies the amount of information shared between two random variables, which are features and their covariance representation in our case. Furthermore, we show *C3R* is permutation invariant, an important property for representing point clouds.

Lemma 1: (Mutual Information Maximization). *C3R* maximises the mutual information \mathbf{I} between \mathbf{F} and \mathbf{C}_{agg} while optimising weights α during training.

Proof: We begin by denoting the mutual information $\mathbf{I}(\mathbf{F}; \mathbf{C}_{\text{agg}})$ as: $\mathbf{I}(\mathbf{F}; \mathbf{C}_{\text{agg}}) = \mathbf{H}(\mathbf{F}) - \mathbf{H}(\mathbf{F}|\mathbf{C}_{\text{agg}})$. The objective is to maximize $\mathbf{I}(\mathbf{F}; \mathbf{C}_{\text{agg}})$, which is equivalent to minimizing the conditional entropy $\mathbf{H}(\mathbf{F}|\mathbf{C}_{\text{agg}})$. The conditional entropy is given by: $\mathbf{H}(\mathbf{F}|\mathbf{C}_{\text{agg}}) = -\mathbb{E}_{\mathbf{F}, \mathbf{C}_{\text{agg}}} [\log p(\mathbf{F}|\mathbf{C}_{\text{agg}})]$. Here, \mathbf{C}_{agg} represents a weighted sum of normalized group covariance matrices. Thus, the optimization of the weights α directly affects the probability distribution $p(\mathbf{F}|\mathbf{C}_{\text{agg}})$.

By optimizing α using Smooth-AP loss [39], we ensure that the probability distribution $p(\mathbf{F}|\mathbf{C}_{\text{agg}})$ is shaped to minimize conditional entropy, thereby maximizing mutual information.

Lemma 2: *C3R* is permutation invariant.

Proof: Let \mathbf{P} be a permutation matrix that permutes the features in \mathbf{F} . The covariance matrix of the permuted features is given by: $\mathbf{C}' = \frac{1}{n-1} (\mathbf{P}\mathbf{F} - \mu') (\mathbf{P}\mathbf{F} - \mu')^\top$, where $\mu' = \frac{1}{n} \sum_{j=1}^n \mathbf{P}\mathbf{F}_j$. Since \mathbf{P} is an orthogonal matrix (i.e., $\mathbf{P}^\top \mathbf{P} = \mathbf{I}$), we have: $\mathbf{C}' = \mathbf{P}\mathbf{C}\mathbf{P}^\top$. All steps in the methodology are invariant to such permutations. Therefore,

the *C3R* preserves permutation invariance, ensuring that \mathbf{C}_{agg} is robust to the ordering of points in the point cloud.

IV. EXPERIMENTAL DESIGN

In this section, we give the details of our datasets and their evaluation protocols. We also discuss the details of our implementation and the evaluation metrics.

A. Datasets

We conduct extensive experiments with four large-scale, public datasets for place recognition (Oxford Robotcar, In-house, MulRan, WildPlaces) to demonstrate the effectiveness of our method. The details are given below.

Oxford Robotcar [3] is the most widely used dataset for LiDAR place recognition. It has LiDAR scans captured by traveling a route of 44 times (≈ 10 km) across Oxford, UK, over a year. The dataset is evaluated by taking the point clouds of one trip as queries and iteratively matched against the point clouds of other trips. In this work, we follow the training and testing splits introduced by Uy et al. [8]. A total of 24.7k point clouds were used for training and testing.

In-house [8] is also a popular dataset in the literature. It has LiDAR scans captured by traveling a route of 5 times (≈ 10 km) across three regions of Singapore – a Business District (B.D.), a Residential Area (R.A.), and a University Sector (U.S.). Similar to the Oxford dataset, we follow the testing split introduced by Uy et al. [8] and use the point clouds from a single trip as queries and the remaining point clouds from other trips as databases iteratively. However, unlike the Oxford dataset, the in-house dataset is only used for testing purposes to demonstrate generalisability. A total of ≈ 4.5 k point clouds were used for testing.

MulRan [4] has LiDAR scans captured by traveling through various urban environments. Among those, we use the traversals of Sejong City (Sejong) and Daejeon Convention Center (DCC) (each 3 runs ≈ 15 km). Following the work of [42], [43], we produce the training and testing splits of both environments and train using only Sejong sequences 1 and 2. The evaluation is done on test sets of both environments.

WildPlaces [5] is a very recent dataset. Unlike the above datasets, it is captured in natural, forest environments. It has LiDAR scans of 33km captured from hiking trails in Brisbane, Australia over 14 months. Following its original paper, we evaluate Venman and Karawatha environments using the inter-sequence training and testing protocol.

B. Implementation details and Evaluation criteria

We implement *C3R* as sandwiched layers using Pytorch and use Adam optimizer. We use a learning rate of 0.0001 and decay it at the end of the learning episode. We use 400 epochs for Oxford following [6] and 100 epochs for MulRan and WildPlaces datasets following [43] and [5], respectively. We use an identical network as Minkloc3Dv2 [6] for obtaining the point cloud features and train using Smooth-AP Loss [39]. All experiments are conducted using a single Nvidia H100 GPU on a HPC cluster.

TABLE I: Evaluation results of Place Recognition methods on Oxford and In-house datasets using the Baseline and Refine Protocols proposed in [8]. The results of existing methods are quoted from original papers while MinkLoc3Dv2 is trained from scratch with the publicly released codebase. R@1: Recall@1; R@1%: Recall@1%.

Method	Pooling	Baseline protocol										Refined protocol									
		Oxford		U.S.		R.A.		B.D.		Avg.	Avg.	Oxford		U.S.		R.A.		B.D.		Avg.	Avg.
		R@1	R@1%	R@1	R@1%	R@1	R@1%	R@1	R@1%	R@1	R@1%	R@1	R@1%	R@1	R@1%	R@1	R@1%	R@1	R@1%	R@1	R@1%
PointNetVLAD [8]	NetVLAD	62.8	83.0	63.2	72.6	56.1	60.3	57.2	65.3	59.8	70.3	63.3	80.1	86.1	94.5	82.7	93.1	80.1	86.5	78.1	88.6
PCAN [20]	NetVLAD	70.3	86.4	73.7	89.1	58.1	69.1	66.8	75.2	67.2	79.9	70.7	86.4	83.7	94.1	82.5	92.5	80.3	87.0	79.3	90.0
LPD-Net [18]	NetVLAD	86.3	94.3	87.0	96.0	79.1	85.7	82.5	89.1	83.7	91.3	86.6	94.9	94.4	98.9	90.8	96.4	90.8	94.4	90.6	96.2
SOE-Net [17]	NetVLAD	89.4	96.5	93.7	96.7	90.2	92.4	-	-	-	-	89.3	96.4	91.8	97.7	90.2	95.9	89.0	92.6	90.1	95.7
MinkLoc3D [25]	GeM	93.0	97.4	86.7	97.5	90.4	91.5	81.5	90.1	87.9	94.1	94.8	98.5	97.2	99.7	96.7	99.3	94.0	96.7	95.7	98.6
PPT-Net [40]	GeM	93.5	97.8	90.1	97.5	89.7	95.1	88.4	90.7	90.4	95.3	-	98.4	-	99.7	-	99.5	-	95.3	-	-
SVT-Net [41]	GeM	95.0	98.5	94.9	97.4	90.4	94.9	89.3	93.3	92.4	96.0	94.7	98.4	97.0	99.9	95.2	99.5	94.4	97.2	95.3	98.8
TransLoc3D [19]	NetVLAD	95.0	98.3	95.4	97.6	91.0	94.7	88.4	94.7	92.5	96.3	95.0	98.5	97.5	99.8	94.4	99.7	94.8	97.4	95.4	98.9
MinkLoc3Dv2 [6]	GeM	95.8	98.7	90.0	96.5	84.9	91.7	84.9	89.7	88.9	94.2	96.8	98.9	98.9	100	98.4	99.7	97.2	98.7	97.8	99.3
Ours	<i>C3R</i>	96.7	98.9	91.5	97.2	86.6	93.3	86.6	90.4	90.4	95.0	97.3	99.0	98.9	100	98.5	99.8	97.8	99.0	98.1	99.5

TABLE II: Evaluation Results with 5m thresholds on Sejong and DCC environments of MulRan dataset using the training and testing protocols proposed in [43]. The results of existing methods are quoted from [43]. R@1: Recall@1; R@5: Recall@5.

Method	Pooling	Sejong		DCC		Average	
		R@1	R@5	R@1	R@5	R@1	R@5
Minkloc3D [25]	GeM	82.3	94.4	63.8	86.7	73.1	90.6
Locus [44]	SoP	67.0	75.8	46.3	55.6	63.1	65.7
PPT-Net [40]	GeM	60.2	76.2	47.9	60.2	56.1	68.2
MinkLoc3Dv2 [6]	GeM	73.1	86.4	62.2	73.2	70.6	80.3
LCD-Net [45]	NetVLAD	63.1	82.0	57.7	71.6	64.3	76.8
Ours	<i>C3R</i>	91.9	97.4	68.6	91.6	80.3	94.5

TABLE III: Evaluation Results on WildPlaces dataset using the training and testing protocols proposed in the dataset [5]. The results of existing methods are quoted from [5]. R@1: Recall@1; MRR: Mean Reciprocal Rank.

Method	Pooling	Venman		Karawatha		Average	
		R@1	MRR	R@1	MRR	R@1	MRR
ScanContext [46]	-	33.98	64.67	38.44	67.90	36.21	66.29
TransLoc3D [19]	NetVLAD	50.24	66.16	46.08	50.24	48.16	58.20
MinkLoc3Dv2 [6]	GeM	75.77	84.87	67.82	79.21	71.80	82.04
LoGG3D-Net [12]	SoP	79.84	87.33	74.67	83.68	77.26	85.51
Ours	<i>C3R</i>	80.22	87.36	75.04	83.73	77.63	85.55

For evaluation, we follow the standard evaluation protocols by PointNetVLAD [8] for the Oxford and In-house datasets, SpectralGV [43] for MulRan dataset and WildPlaces [5] for natural dataset. For comparisons, we use the commonly used average recall (AR)@N (*i.e.*, AR@1 and AR@1%) and MRR (mean reciprocal rank).

V. RESULTS

In this section, we discuss our experimental results. We also provide an ablation study of various first and second-order pooling methods, and the partition sizes of *C3R*.

A. Comparison with state-of-the-art methods

We compare the performance of our optimal *C3R* model trained using the setting (*i.e.*, protocols and evaluation criteria) mentioned in Section IV-B with the state-of-the-art methods on place recognition using different datasets.

Table I shows the comparisons of results on Oxford and In-house datasets using both baseline and refined protocols. We compare our results with PointNetVLAD [8], PCAN [20], LPD-Net [18], SOE-Net [17], Minkloc3D [25], PPT-Net [40], SVT-Net [41], TransLoc3D [19] and Minkloc3Dv2 [6]. The results show that our methods achieve the best

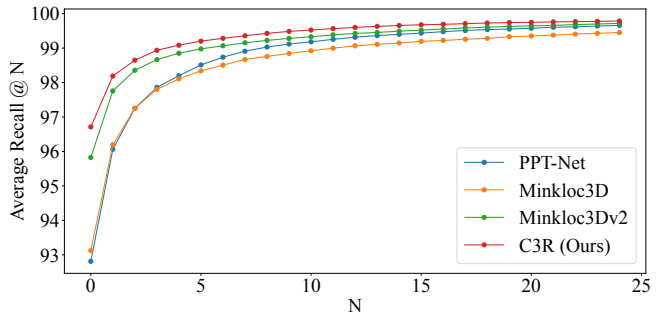


Fig. 3: Average recall @N on the Oxford Robocar dataset. Our method can reliably retrieve the position of query point clouds in a given database than the other methods.

performance in terms of both R1 and R1% under the Refined protocol. Under the baseline protocol, we perform best in the Oxford case and comparably with the other methods. Minkloc3Dv2 is the closest method to ours since we only differ with it in terms of the pooling method. In that, we can see a clear indication of performance improvement of *C3R*. In Fig. 3, compare our recall rates with PPT-Net, Minkloc3D, and Minkloc3Dv2 methods. It shows that we consistently outperform them through different recall rates. It is worth mentioning that the Oxford and In-house datasets only contain approx. 4k points per point cloud frames which limits the information retrieval capacity of more advanced pooling mechanisms such as ours.

Next, we compare our results on a more complex LPR task on MulRan dataset. Table II shows the results. We compare with Minkloc3D [25], Locus [44], PPT-Net [40], MinkLoc3Dv2 [6] and LCD-Net [45]. The results show that the *C3R* significantly outperforms the existing methods by a large margin on both Sejong and DCC sequences across R1 and R5. Note that the MulRan dataset has a comparably complex scene structure and DCC sequences are unseen during training, therefore, our SOTA results on DCC suggest that the *C3R* has a powerful generalization ability in complex scenes.

Finally, we evaluate our results on the WildPlaces dataset using the intra-sequence protocol. Table III shows the result. We compare with ScanContext [46], TransLoc3D [19], MinkLoc3Dv2 [6] and LoGG3D-Net [12]. The results show that our method surpasses the performance of the existing methods on both environments (Venman, Karawatha). In

TABLE IV: Comparison with various pooling methods on Oxford and In-house datasets using baseline protocol [6]. All methods are computed using 256 feature channels. Bold-face results indicate improvements over first-order pooling methods on the top part of the table.

Method	Oxford		U.S.		R.A.		B.D.		Dim	Retrieval Time (mins)
	R@1	R@1%	R@1	R@1%	R@1	R@1%	R@1	R@1%		
Existing pooling mechanisms used for LiDAR place recognition										
GAP [7]	90.7	97.4	81.4	91.3	76.1	86.9	77.4	85.0	256	2.89
GMP [7]	93.9	98.1	87.0	94.9	78.7	88.9	80.7	86.8	256	3.10
NetVLAD [23]	93.5	98.2	86.3	94.9	81.9	91.1	82.5	88.7	256	4.52
GeM [7]	95.8	98.7	90.0	96.5	84.9	91.7	84.9	89.7	256	3.03
iSQRT-COV [13]	97.4	99.1	93.9	98.7	92.1	96.4	90.5	93.6	32k	18.9
CBP [9]	90.6	96.9	78.7	88.9	77.1	88.9	77.3	83.9	8k	6.03
SoP [12]	95.3	98.7	86.2	93.2	92.2	98.2	86.1	90.3	64k	37.6
<i>C3R (Ours)</i>										
<i>C3R (k = 2)</i>	96.7	98.9	91.5	97.2	86.6	93.3	86.6	90.4	8k	5.93
<i>C3R (k = 4)</i>	95.9	98.7	90.7	97.2	83.7	91.1	83.8	88.5	2k	4.40
<i>C3R (k = 8)</i>	94.9	98.5	86.9	94.3	80.8	90.9	81.5	86.7	528	3.45
<i>C3R (k = 16)</i>	92.0	97.9	83.7	94.0	78.1	88.5	79.8	86.5	126	2.03

comparison with LoGG3D-Net, our method uses an ordinary loss and encoder network and trains 2x faster on a single GPU.

B. Ablation study

To show that *C3R* is better than the existing pooling method, we compare its performance with the existing pooling techniques used across various LPR methods in the literature. Specifically, we compare five popular first-order pooling methods, namely, global average pooling (GAP), global max pooling (GMP), NetVLAD [23], Generalised mean pooling (GeM) [7], two popular full covariance based second-order pooling methods, namely, iSQRT-COV [13] and Second-order pooling (SoP) [12] and compact bilinear pooling (CBP) [9]. We chose the baseline protocol used in [6] for this experiment as it has been extensively used across the literature. Table IV shows the results of the comparison.

The top part of the table compares the performance of various first-order pooling methods. It is clear to see that iSQRT-COV surpasses the performance of first-order pooling methods. Interestingly, it also exceeds the performance of CBP and HoP. However, it has a significantly high dimension. We use the output size of 8k in the case of CBP following the original paper for better performance.

The bottom part of the table shows the performance of our *C3R*. Clearly, our *C3R* variant with $k = 2$ and $k = 3$ achieves better performance than the CBP and SoP in most cases. Note that the baseline protocol trains only on the Oxford dataset and evaluates the In-house datasets which gives an understanding of feature generalisation. Therefore, it is evident that *C3R* also improves the feature generalization ability in comparison with the methods on the top part of the table. Furthermore, it produces significantly smaller feature dimensions than the CBP and SoP, improving the retrieval time as shown in the last column of the table.

C. Quantitative results

In Fig. 4, we provide some quantitative results for a deeper understanding of our *C3R* and an understanding of LPR. We compare the feature descriptors of the query point cloud produced by our method with the ones stored in the database. The point clouds that match with the database are denoted with a green box and the ones that are denoted

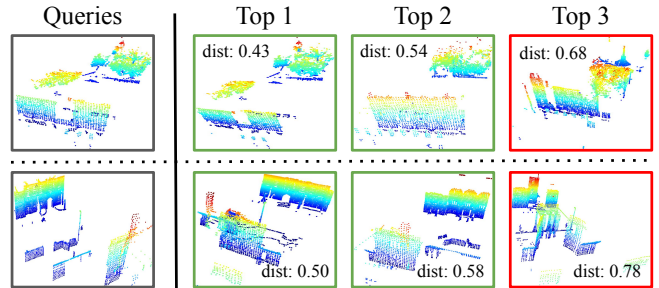


Fig. 4: Top-3 database results for the provided query point clouds. The green border denotes a correct match while red border is from a different place. The Euclidean distance between the query and database descriptors is shown. It is noticeable that the matched point clouds are visually similar and have lower distances compared to unmatched ones.

with a red box are from different locations. We can see that the query is successfully retrieved in the top 1. The top 2 are also from the same location, while the third is from a different location. The failure of the top 3 in the top row is due to the subtle spatial difference in the middle while the bottom row is due to their major structural dissimilarity. Furthermore, we can notice the top 1 and 2 have less distance with the query compared to the top 3 retrieval.

VI. CONCLUSION

This paper proposes a compact covariance pooling method called *C3R* for learning effective feature channel correlations with end-to-end models for LPR. It improves the shortcomings of traditional covariance pooling methods in terms of their high dimensions, which affects the efficiency of database retrieval in LPR. It has negligible learnable parameters compared to popular methods such as NetVLAD, reducing the risk of overfitting in low-data regimes. We conducted extensive experiments on four popular LPR datasets to demonstrate the effectiveness of *C3R*. Experimental results reveal state-of-the-art (SOTA) results on all four datasets. Specifically, it achieved an R@1 score of 91.9% (Sejong) and 68.6% (DCC) on the MulRan dataset, significantly outperforming existing methods using similar backbones and training mechanisms. It also achieved SOTA results on the WildPlaces dataset across both environments. We also provide quantitative results of our method and compare its performance with existing methods in terms of varying recall rates to better understand its reliability. In the ablation study, we compare various pooling methods, demonstrating that our method outperforms popular pooling methods in LPR.

ACKNOWLEDGEMENTS

This work was partially funded by the CSIRO's Machine Learning and Artificial Intelligence (MLAI) FSP and CSIRO's Data61 Science Digital.

REFERENCES

- [1] C. Cadena, L. Carlone *et al.*, “Past, present, and future of simultaneous localization and mapping: Toward the robust-perception age,” *IEEE Transactions on robotics*, vol. 32, no. 6, pp. 1309–1332, 2016.
- [2] C. Park, P. Moghadam *et al.*, “Elasticity meets continuous-time: Map-centric dense 3D LiDAR SLAM,” *IEEE Transactions on Robotics*, vol. 38, no. 2, pp. 978–997, 2021.
- [3] W. Maddern, G. Pascoe *et al.*, “1 year, 1000 km: The oxford robotic dataset,” *IJRR*, vol. 36, no. 1, pp. 3–15, 2017.
- [4] G. Kim, Y. S. Park *et al.*, “Mulran: Multimodal range dataset for urban place recognition,” in *ICRA*. IEEE, 2020, pp. 6246–6253.
- [5] J. Knights, K. Vidanapathirana *et al.*, “Wild-Places: A Large-Scale Dataset for Lidar Place Recognition in Unstructured Natural Environments,” in *2023 IEEE International Conference on Robotics and Automation (ICRA)*, 2023, pp. 11 322–11 328.
- [6] J. Komorowski, “Improving point cloud based place recognition with ranking-based loss and large batch training,” in *2022 26th International Conference on Pattern Recognition (ICPR)*. IEEE, 2022, pp. 3699–3705.
- [7] F. Radenović, G. Tolias *et al.*, “Fine-tuning cnn image retrieval with no human annotation,” *T-PAMI*, vol. 41, no. 7, pp. 1655–1668, 2018.
- [8] M. A. Uy and G. H. Lee, “Pointnetvlad: Deep point cloud based retrieval for large-scale place recognition,” in *CVPR*, 2018, pp. 4470–4479.
- [9] Y. Gao, O. Beijbom *et al.*, “Compact bilinear pooling,” in *CVPR*, 2016, pp. 317–326.
- [10] T.-Y. Lin and S. Maji, “Improved bilinear pooling with cnns,” *arXiv preprint arXiv:1707.06772*, 2017.
- [11] J. Zhang, Z. Zhang *et al.*, “Kernel-based feature aggregation framework in point cloud networks,” *Pattern Recognition*, vol. 139, p. 109439, 2023.
- [12] K. Vidanapathirana, M. Ramezani *et al.*, “LoGG3D-Net: Locally guided global descriptor learning for 3D place recognition,” in *ICRA*. IEEE, 2022, pp. 2215–2221.
- [13] P. Li, J. Xie *et al.*, “Towards faster training of global covariance pooling networks by iterative matrix square root normalization,” in *CVPR*, 2018, pp. 947–955.
- [14] S. Hausler, S. Garg *et al.*, “Patch-netvlad: Multi-scale fusion of locally-global descriptors for place recognition,” in *Proceedings of the IEEE/CVF conference on computer vision and pattern recognition*, 2021, pp. 14 141–14 152.
- [15] A. Ali-Bey, B. Chaib-Draa *et al.*, “Mixvpr: Feature mixing for visual place recognition,” in *Proceedings of the IEEE/CVF winter conference on applications of computer vision*, 2023, pp. 2998–3007.
- [16] S. Izquierdo and J. Civera, “Optimal transport aggregation for visual place recognition,” in *Proceedings of the IEEE/CVF Conference on Computer Vision and Pattern Recognition*, 2024, pp. 17 658–17 668.
- [17] Y. Xia, Y. Xu *et al.*, “Soe-net: A self-attention and orientation encoding network for point cloud based place recognition,” in *Proceedings of the IEEE/CVF Conference on computer vision and pattern recognition*, 2021, pp. 11 348–11 357.
- [18] Z. Liu, S. Zhou *et al.*, “Lpd-net: 3d point cloud learning for large-scale place recognition and environment analysis,” in *Proceedings of the IEEE/CVF International Conference on Computer Vision*, 2019, pp. 2831–2840.
- [19] T.-X. Xu, Y.-C. Guo *et al.*, “Transloc3d: Point cloud based large-scale place recognition using adaptive receptive fields,” *arXiv preprint arXiv:2105.11605*, 2021.
- [20] W. Zhang and C. Xiao, “Pcan: 3d attention map learning using contextual information for point cloud based retrieval,” in *Proceedings of the IEEE/CVF Conference on Computer Vision and Pattern Recognition*, 2019, pp. 12 436–12 445.
- [21] L. Wiesmann, R. Marcuzzi *et al.*, “Retriever: Point cloud retrieval in compressed 3d maps,” in *ICRA*. IEEE, 2022, pp. 10925–10932.
- [22] L. Wiesmann, L. Nunes *et al.*, “Kppr: Exploiting momentum contrast for point cloud-based place recognition,” *IEEE Robotics and Automation Letters*, vol. 8, no. 2, pp. 592–599, 2022.
- [23] R. Arandjelovic, P. Gronat *et al.*, “Netvlad: Cnn architecture for weakly supervised place recognition,” in *CVPR*, 2016, pp. 5297–5307.
- [24] C. R. Qi, H. Su *et al.*, “Pointnet: Deep learning on point sets for 3d classification and segmentation,” in *CVPR*, 2017, pp. 652–660.
- [25] J. Komorowski, “Minkloc3d: Point cloud based large-scale place recognition,” in *WACV*, 2021, pp. 1790–1799.
- [26] J. Knights, S. Hausler *et al.*, “GeoAdapt: Self-supervised test-time adaptation in lidar place recognition using geometric priors,” *IEEE Robotics and Automation Letters*, vol. 9, no. 1, pp. 915–922, 2024.
- [27] T. Barros, L. Garrote *et al.*, “Attdlnet: Attention-based deep network for 3d lidar place recognition,” in *Iberian Robotics conference*. Springer, 2022, pp. 309–320.
- [28] H. Lai, P. Yin *et al.*, “Adafusion: Visual-lidar fusion with adaptive weights for place recognition,” *IEEE Robotics and Automation Letters*, vol. 7, no. 4, pp. 12 038–12 045, 2022.
- [29] P. Koniusz, H. Zhang *et al.*, “A deeper look at power normalizations,” in *CVPR*, 2018, pp. 5774–5783.
- [30] P. Koniusz and H. Zhang, “Power normalizations in fine-grained image, few-shot image and graph classification,” *IEEE Transactions on Pattern Analysis and Machine Intelligence*, vol. 44, no. 2, pp. 591–609, 2021.
- [31] T.-Y. Lin, A. RoyChowdhury *et al.*, “Bilinear cnn models for fine-grained visual recognition,” in *Proceedings of the IEEE international conference on computer vision*, 2015, pp. 1449–1457.
- [32] P. Li, J. Xie *et al.*, “Is second-order information helpful for large-scale visual recognition?” in *CVPR*, 2017, pp. 2070–2078.
- [33] T. Yu, Y. Cai *et al.*, “Efficient compact bilinear pooling via kronecker product,” in *Proceedings of the AAAI Conference on Artificial Intelligence*, vol. 36, no. 3, 2022, pp. 3170–3178.
- [34] K. Vidanapathirana, P. Moghadam *et al.*, “Locus: Lidar-based place recognition using spatiotemporal higher-order pooling,” in *ICRA*. IEEE, 2021, pp. 5075–5081.
- [35] H. Jégou, M. Douze *et al.*, “On the burstiness of visual elements,” in *2009 IEEE conference on computer vision and pattern recognition*. IEEE, 2009, pp. 1169–1176.
- [36] M. Engin, L. Wang *et al.*, “Deepkspd: Learning kernel-matrix-based spd representation for fine-grained image recognition,” in *Proceedings of the European Conference on Computer Vision (ECCV)*, 2018, pp. 612–627.
- [37] N. Higham, “Functions of matrices: Theory and computation,” 2008.
- [38] C. Yu, X. Zhao *et al.*, “Hierarchical bilinear pooling for fine-grained visual recognition,” in *Proceedings of the European conference on computer vision (ECCV)*, 2018, pp. 574–589.
- [39] A. Brown, W. Xie *et al.*, “Smooth-ap: Smoothing the path towards large-scale image retrieval,” in *European conference on computer vision*. Springer, 2020, pp. 677–694.
- [40] Z. Zhou, C. Zhao *et al.*, “Ndt-transformer: Large-scale 3d point cloud localisation using the normal distribution transform representation,” in *2021 IEEE International Conference on Robotics and Automation (ICRA)*. IEEE, 2021, pp. 5654–5660.
- [41] Z. Fan, Z. Song *et al.*, “Svt-net: Super light-weight sparse voxel transformer for large scale place recognition,” in *Proceedings of the AAAI Conference on Artificial Intelligence*, vol. 36, no. 1, 2022, pp. 551–560.
- [42] J. Komorowski, M. Wysoczanska *et al.*, “Egonn: Egocentric neural network for point cloud based 6dof relocation at the city scale,” *IEEE Robotics and Automation Letters*, vol. 7, no. 2, pp. 722–729, 2021.
- [43] K. Vidanapathirana, P. Moghadam *et al.*, “Spectral Geometric Verification: Re-Ranking Point Cloud Retrieval for Metric Localization,” *IEEE Robotics and Automation Letters*, vol. 8, no. 5, pp. 2494–2501, 2023.
- [44] —, “Locus: LiDAR-based Place Recognition using Spatiotemporal Higher-Order Pooling,” in *IEEE International Conference on Robotics and Automation (ICRA)*, 2021.
- [45] D. Cattaneo, M. Vaghi *et al.*, “Lcdnet: Deep loop closure detection and point cloud registration for lidar slam,” *IEEE Transactions on Robotics*, vol. 38, no. 4, pp. 2074–2093, 2022.
- [46] G. Kim and A. Kim, “Scan context: Egocentric spatial descriptor for place recognition within 3d point cloud map,” in *IROS*. IEEE, 2018, pp. 4802–4809.